physica status solidi b
www.pss-b.com
basic solid state physics

The effect of interstitial hydrogen on the electronic structure of the B2 FeAl alloy

Estela A. González[1], **Paula V. Jasen**[1], **Graciela Brizuela**[1, 2], **Alfredo Juan**[1, 2], and **Risto Nieminen**[2]

[1] Departamento de Física, Universidad Nacional del Sur, Av. Alem 1253, Bahía Blanca (8000), Argentina
[2] Laboratory of Physics, Helsinki University of Technology, P.O. Box 1100, 02015 HUT, Finland

Received 17 February 2007, revised 30 May 2007, accepted 20 June 2007
Published online 3 August 2007

PACS 71.15.Ap, 71.15.Mb, 71.20.Be, 71.20.Eh, 71.55.Ak

The electronic structure and bonding in a B2 Fe–Al alloy with and without hydrogen as an interstitial atom were studied within the framework of the density functional theory and the findings compared with previous results in Fe an Al. The hydrogen absorption turns out to be a favorable process. The hydrogen was found near an Al octahedral site, the Al–H distance being shorter than that of Fe–H. The density of states (DOS) curves show several peaks below the d metal band which is made up mostly of hydrogen based states (>50% H_{1s}) while the metal contribution includes mainly s- and p-orbitals. An electron transfer of nearby 0.14 e^- comes from the metal to the H. The overlap population values reveal metal–metal bond breaking, the intermetallic bond being the most affected. The H bond mainly with the Al atoms and the reported Fe–H overlap population is much lower than that corresponding to FePd alloys and BCC Fe. The changes in the overlap population show the Fe–Al bond is weakening nearly 53% after H absorption, while the Fe–Fe bond is only weakened 23%.

phys. stat. sol. (b) **244**, No. 10, 3684–3694 (2007) / **DOI** 10.1002/pssb.200743076

physica status solidi b

phys. stat. sol. (b) **244**, No. 10, 3684–3694 (2007) / **DOI** 10.1002/pssb.200743076

The effect of interstitial hydrogen on the electronic structure of the B2 FeAl alloy

Estela A. González[1], **Paula V. Jasen**[1], **Graciela Brizuela**[1, 2], **Alfredo Juan**[*, 1, 2], and **Risto Nieminen**[2]

[1] Departamento de Física, Universidad Nacional del Sur, Av. Alem 1253, Bahía Blanca (8000), Argentina
[2] Laboratory of Physics, Helsinki University of Technology, P.O. Box 1100, 02015 HUT, Finland

Received 17 February 2007, revised 30 May 2007, accepted 20 June 2007
Published online 3 August 2007

PACS 71.15.Ap, 71.15.Mb, 71.20.Be, 71.20.Eh, 71.55.Ak

The electronic structure and bonding in a B2 Fe–Al alloy with and without hydrogen as an interstitial atom were studied within the framework of the density functional theory and the findings compared with previous results in Fe an Al. The hydrogen absorption turns out to be a favorable process. The hydrogen was found near an Al octahedral site, the Al–H distance being shorter than that of Fe–H. The density of states (DOS) curves show several peaks below the d metal band which is made up mostly of hydrogen based states (>50% H_{1s}) while the metal contribution includes mainly s- and p-orbitals. An electron transfer of nearby 0.14 e^- comes from the metal to the H. The overlap population values reveal metal–metal bond breaking, the intermetallic bond being the most affected. The H bond mainly with the Al atoms and the reported Fe–H overlap population is much lower than that corresponding to FePd alloys and BCC Fe. The changes in the overlap population show the Fe–Al bond is weakening nearly 53% after H absorption, while the Fe–Fe bond is only weakened 23%.

1 Introduction

The physicochemical mechanisms of bonding in iron aluminides have attracted renewed attention. Yield strength anomaly, vacancy hardening, and the effect of alloying elements on hydrogen embrittlement have stimulated interest in this subject. Consequently, these effects open new fields of applications for iron aluminides. A clear understanding of the mechanical, electrical, and thermodynamic properties of alloyed iron aluminides require the study of the features of metal-metal bonding in these alloys, doped by other elements [1].

The nature of bonding in alloyed FeAl (B2 phase) determines the structure of compounds and the distribution of alloying atoms on the sublattices. Intermetallic compounds based on the B2 FeAl phase have been widely investigated because of their important physical and mechanical properties [2–7]. The mechanical characteristics of intermetallics are usually improved by alloying [8, 9]. It is necessary to understand the properties of the alloys at the microscopic level and to elucidate the peculiarities of the electron structure and the nature of bonding in the intermetallics with the ternary additives. Both chemical bonding and site preference occupation of transition metal (TM) in Fe–Al result from chemical properties of the TM, which determine the atomic coordination according to the Pauling concept [10].

* Corresponding author: e-mail: cajuan@uns.edu.ar, Fax: 54-291-4595142
Present address: Dpt. of Mechanics and Aerospace Eng., Princeton University, Princeton, NJ 08540, USA

Numerous technological applications require the use of intermetallic alloys. Changing the intermetallic alloys stoichiometry and their crystal structures can yield new materials relatively easily. One goal of this research is to find an alloy, which remains strong at high temperatures yet, ductile at low temperatures. Of particular interest are TM aluminides, e.g. FeAl, NiAl, and CoAl, which are resistant to corrosion and oxidation, have interesting magnetic properties, and are used as high temperature structural materials and soft magnetic materials [11]. First-principles calculations can be used as an aid in developing new alloys of this type. The determination of other properties, e.g. surface interface energies and dislocations energies, are at best at the cutting edge of computational physics [12].

Due to their appealing high-temperature and corrosion resistance properties, intermetallic alloys are the subjects of an increasing amount of studies. Nevertheless, their mechanical behavior is not fully understood up to now: in particular, their strong room temperature intergranular brittleness, impairing their industrial use as structural materials, has neither been satisfactorily explained nor remedied [13].

Such a complex phase diagram describes the Fe–Al system that is totally hopeless to attempt to determine a potential whose reliability would extend over the whole range of compositions. B2 FeAl possesses hardly understood mechanical properties. This ordered phase, according to diffraction data, exists between 38 and 52 at% Al in a wide range of temperatures and concentrations. However, in order to be efficient in the study of segregations processes at interfaces, this description should also take into account the pure elements [14].

There are an interesting number of theoretical studies on intermetallic alloys [14–26]. Zou and Fu have shown that the dominant factor for early TM aluminides is the directional bonding between the d-orbital of TM atoms, whereas for late TM aluminides, charge transfer and hybridization between Al sp and TM d-states play more important roles in the bonding [16].

Theoretical calculations have been compared with experimental data by Schott and Fähnle [18] and by Bogner et al. [19]. The electronic structure of iron aluminides has also been computed using clusters and extended structures of variable Al composition [20–23]. Recently, density functional theory (DFT) in the local density approximation with the Hubard Hamiltonian (LDA + U) [24] and accurate tight-binding (TB) parameterization of LDA schemes yield a non-magnetic ground state for B2 FeAl [24, 25]. The difficulties to reproduce experimental ground states for FeAl and Fe_3Al have been pointed out by Lechermann et al. [26].

A study combining ab initio electron theory and statistical mechanics, using the new Stuttgart ab initio mixed-basis pseudopotential code in the generalized gradient approximation (GGA) has calculated the ternary phase diagram for Ni–Al–Fe [27]. Fähnle et al. have published an interesting review article on DTF calculations for single defects in B2 FeAl [28].

DFT has been used to study the behavior of single defects in B2-FeAl-vacancies, as well as boron, carbon, nitrogen, and oxygen substituting for Fe or Al atoms [29].

As mentioned before, the FeAl alloys have been the subjects of several theoretical publications; however its interaction with H is not fully understood. The thermodynamics and solubility of hydrogen in FeAl have been measured in the range 513–1301 K by Xu and McLellan [30].

To the best of our knowledge there are only a few theoretical studies on the effect of H in B2 FeAl alloy. The environmental embrittlement in FeAl alumninides has been reviewed by Liu et al. [31]. The DFT calculations of Fu and Painter have predicted that H dilates the Fe–Al lattice and decreases its cohesive strength when H is absorbed in Fe-rich sites [32]. Fu and Wang have studied the effect or ordering, vacancies and the mechanism underlying the hydrogen-induced embrittlement effect. These authors have found hydrogen located at the tetrahedral sites with and Fe–H distance of 1.55 Å with a decrease in the Fe d charge along the Fe–H direction on Fe sites [33].

The investigation of the band structure is also important to reveal the origin of chemical bonding in Fe–Al alloys and its interaction with H as an impurity in extended structures. The present calculations were performed using the package ADF-BAND a density functional method. Due to the low mass of hydrogen, the zero-point (ZP) vibrational energy of H in the hydrides may be important and contribute to the absorption energy [34, 35]. Ke et al. have performed quantum mechanical calculations on the ZP vibrations of H in octahedral sites of metal hydrides by solving the time-independent Schrödinger equa-

tion based on a three-dimensional adiabatic potential [36]. In Fe-based systems our estimation of ZP introduces a correction of about 0.10 eV/atom [37]. After a brief description of the model, we report the electronic structure and bonding on B2 Fe–Al alloy in a ordered bulk structure. The effect of incorporating H as an impurity on the Fe–Fe, Al–Al and Fe–Al bonding is also addressed.

2 Computational method

Gradient-corrected density functional theory (GC-DFT) calculations were performed on a supercell containing 108 atomic sites in a cubic lattice (B2-phase) to model bulk FeAl, with a $4 \times 4 \times 4$ reciprocal space grid in the supercell Brillouin zone and a plane-wave kinetic energy cutoff of 220 eV for the Fe–Al–H system [38–40]. We used the Amsterdam Density Functional 2000 package (ADF-BAND2000) [41]. The molecular orbitals were represented as linear combinations of Slater functions. The gradient correction the Becke [42] approximation for the exchange energy functional and the B3LYP [43] approximation for the correlation functional were employed. In order to increase the computational efficiency, the innermost atomic shells of electrons are kept frozen for every atom except hydrogen, since the internal electrons do not contribute significantly to the bonding. We have used a triple-zeta basis set (this means three Slater-type functions for each atomic valence orbital occupied) with polarization functions to express the atomic orbitals of Fe and Al. The basis set of Fe consisted of 3p-, 3d- and 4s-orbitals and for Al 3s and 3p. With this set we obtained a magnetic moment of $2.26\mu_B$ for BCC Fe, which compares very well with the experimental value of $2.20\mu_B$. To understand the Fe–Al–H interactions we used the concept of density of states (DOS) and overlap population density of states (OPDOS). The DOS curve is a plot of the number of orbitals as a function of the energy. The integral of the DOS curve over an energy interval gives the number of one-electron states in that interval; the integral up to the Fermi level (E_F) gives the total number of occupied molecular orbitals. If the DOS is weighed with the overlap population between two atoms the overlap population density of states OPDOS is obtained. The integration of the OPDOS curve up to E_F gives the total overlap population of the specified bond orbital and it is a measure of the bond strength. If an orbital at certain energy is strongly bonding between two atoms the overlap population is strongly positive and OPDOS curve will be large and positive around that energy. Similarly, OPDOS negative around a certain energy corresponds to antibonding interactions.

The irreducible wedge of the Brillouin zone was defined by $0 \le k_a \le \pi/2$, $0 \le k_b \le \pi/2$, $0 \le k_c \le \pi/2$. The k-points set were generated according to the geometrical method of Ramirez and Böhm [44, 45]. The symmetry lines $\Gamma \rightarrow X$; $X \rightarrow W$; $W \rightarrow L$; $L \rightarrow \Gamma$ along the crystal were used to calculate the band structure.

The absorption energy was computed as the difference ΔE between the Fe–Al–H composite system when the H atom is absorbed at its minima location geometry and when it is far away from the Fe–Al alloy. It can be expressed as

$$\Delta E_{\text{Total}} = E(\text{FeAlH}) - (E(\text{FeAl}) + E(\text{H})),$$

where E is the electronic energy, $E(\text{FeAl})$ corresponds to the pure alloy.

3 Crystal structure

In the range 0–50 at% Al, the structural changes connect a disorder → order transformation $\alpha \rightarrow Fe_3Al$ ($\beta 1$) and $\alpha \rightarrow$ FeAl ($\beta 2$). The first indication of the occurrence of a transformation in the α solid solution was the detection of an ordered body cubic centered (BCC) structure of CsCl (B2) type [46]. The existence of two superlattices based on the ideal composition $Fe_3Al = \beta 1$ and FeAl = $\beta 2$ were established by Ekman [47], Bradley and Jay [48, 49] in the early 1930's. The Fe_3Al superlattice is formed below 600 °C, whereas the FeAl superlattice is stable up to 700 °C; however, the formation of the latter superlattice might not be suppressed by quenching. The transition of one type of structure to the other is continuous. The B2 Fe–Al phase has a lattice parameter $a_0 = 2.90$ Å [15]. The crystal structure is shown in Fig. 1a.

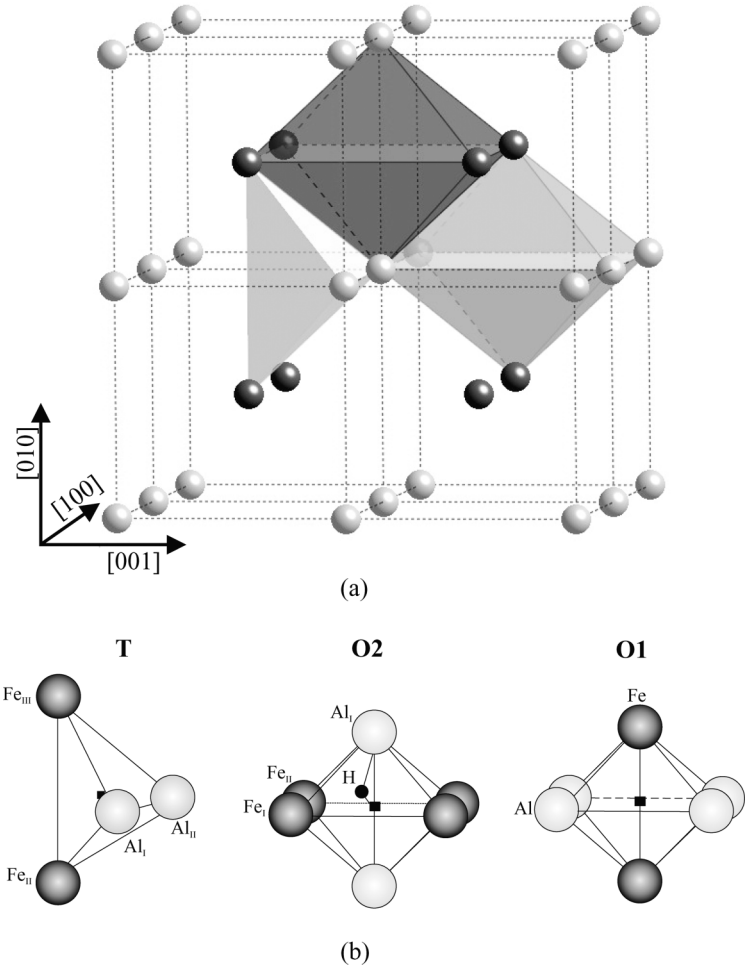

Fig. 1 Crystal structures for the B2 FeAl alloy (a). Schematic view of interstitial sites indicated by a black square (T: tetrahedral, O1: octahedral with Al atoms in its base and O2: octahedral with Fe atoms in its base) (b). The small black circle indicates the energetic minima for H. ● Fe, ● Al, ● H.

We have studied the H absorption on the B2 FeAl phase alloy structure using a supercell of 108 atoms. The B2 FeAl structure have three types of interstitial sites, one tetrahedral (T) and two octahedral (O1, O2). All tetrahedral are equivalent with the same chemical environment around the site (see Fig. 1b, left). The O2 is an octahedral formed by four iron atoms in its base capped with two aluminum atoms (see Fig. 1b, middle) while the O1 has four aluminum atoms in its base capped with two iron atoms (see Fig. 1b, right). After the energy minimization, the H was found near the O2 octahedral site (0.54 Å). Figure 1b shows the final location of the H atom. We have also computed the energetic of the diffusion from a *T* to an octahedral site.

4 Results and discussion

4.1 Pure Fe–Al alloys

Let us first calculate the electronic structure of pure Fe–Al alloys. Figure 2a shows the Total DOS for the B2 FeAl structure. The DOS is similar to that reported previously [15–25, 50–56]. First principles

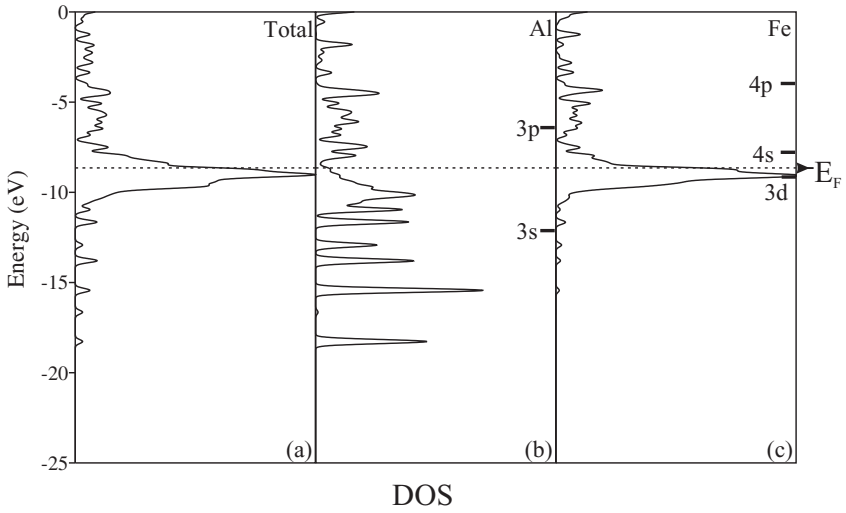

Fig. 2 Total DOS curves for the B2 FeAl alloy (a). Projected DOS on an Al atom (b) and on a Fe atom (c). The bars on the right of (b) and (c) indicate the Al and Fe atomic levels. (The DOS plot for Al has been amplified for a better viewing.)

calculations [54, 57] have pointed out to the formation of a pseudo band gap at the top of the 3d-band [23, 58, 59]. The d-bandwidth is 3.6 eV, which corresponds to the extension of the Fe states while Al based states contribute much less, showing several peaks. Near the Fermi level there is also a peak centered at −10.2 eV somewhat dispersed and corresponds to Al p-states (see Fig. 2b). Similar results for Al and Fe orbital projected DOS were found by Reddy et al. [20]. If we look at the detailed composition of, say, the Fe in the unit cell we obtain the orbital populations $d^{8.24}$ $s^{0.59}$ $p^{0.12}$. Note than on average any Fe atom has its s-band approximately 23% filled.

The Al orbital composition is $s^{1.07}$ $p^{1.21}$ $d^{0.00}$. The importance of Al to TM charge transfer and the filling of the d-band require that a late TM atom has as many Al atoms as its nearest neighbors as possible to facilitate the charge transfer and bonding hybridization [16, 19]. A strong hybridization between Al sp-states and Fe d-states has been reported in [19, 55], leading to a partly covalent character of the bond [60].

Regarding the bonding, the OPDOS curves in Fig. 3 show almost all bonding regions. However, near to the Fermi level (E_F) the Fe–Fe interaction is antibonding. The Fe–Al, the Fe–Fe and the Al–Al OP have similar numerical values (see Table 1). Reddy et al. mentioned that the conduction band approaches very close to the Fermi level and is mainly composed of hybridized Al sp–Fe d levels [20]. In Table 1, the valence orbital occupations, overlap populations and distances are summarized.

Recently Börnsen et al. have published an analysis of the electronic structure of intermetallic compounds in B2-phase. They tested the general assumption that in the B2-phases TMAl the default energetic may be mainly traced back to the properties of the TM-d–Al-sp bonds. The authors conclude that the s-orbitals of the Al atoms donate about one electron to the orbitals of the TM atom. Also the d-orbitals of the TM atoms carry about 1.7 electrons more than in the free atom [61].

4.2 Hydrogen absorption

The hydrogen absorption in the FeAl alloy is a favorable process. The H atom usually occupies interstitial sites in pure metals and alloys. As mentioned in the crystal structure section, the octahedral interstitial sites are non-equivalent. In addition, previous literature results are not definitive [32, 33]. Fu and Paintier absorbe H at the tetrahedral site, however, not full geometry optimization was performed [32]. Fu and Wang found the H located at tetrahedral sites with a Fe–H distance of 1.55 Å, which is close to

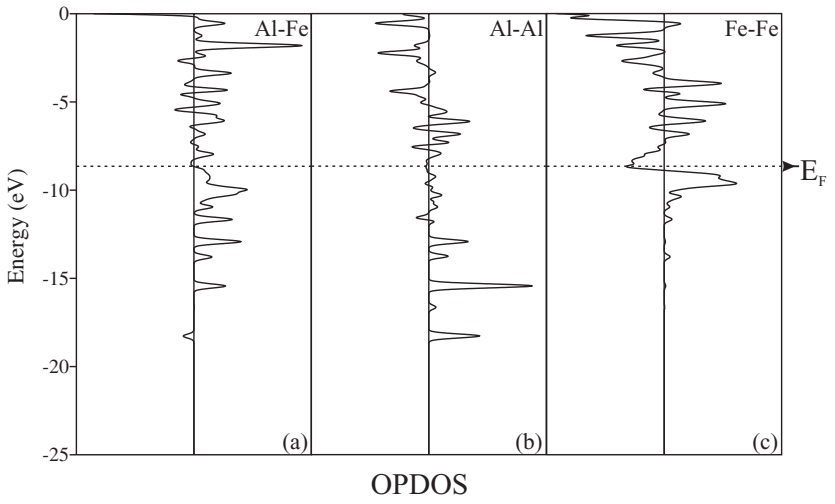

Fig. 3 OPDOS curves of the B2 FeAl alloy: Al–Fe first neighbors (a), Al–Al (b) and Fe–Fe (c).

the geometrical center of the tetrahedral interstitial site (1.623 Å). Studying the redistribution of the electronic density on the (100) atomic plane, with H absorbed in the interstitial site of FeAl, Fu and Wang report a similar decrease of the d charge on the Fe–H directions although the H bonding site is different from that of their previous studies [33]. The two types of octahedral sites mentioned before were not previously considered in detail. The tetrahedral locations for H are –1.75 eV more stable than O1 but +0.93 eV less stable than at the O2 site. Following a similar procedure than that reported by Jiang and Carter [37] we have computed an energy profile for H diffusion from one T-site to a nearest-neighbour O2 site.

The computed Fe–H minimum distance is 1.746 Å at O2, which is somewhat longer than that obtained for FeAl alloys when H is located at the tetrahedral site [33]. The Al–H distance at O2 is 1.166 Å, which is shorter than that reported by Lu and Kaxiras when hydrogen is close to an Al vacancy in pure aluminum [62]. Regarding the electronic structure after H absorption, the DOS shows additional peaks

Table 1 Valence occupations, overlap population, charge (Mulliken's gross charge) and distances for Fe–Al B2 alloy with H absorbed at O2.

structure	occupation			charge	bond type	OP[1]	Δ(OP)[2]	distance (Å)
	s	p	d					
Fe–Al								
Al_I	1.07	1.21	0.00	–0.949	Al_I–Al_{II}	0.231	–	2.904
Fe_I	0.59	0.12	8.21	–0.949	Fe_I–Fe_{II}	0.199	–	2.904
					Fe_{II}–Al_I	0.292	–	2.515
Fe–Al–H								
H	1.13	0.00	0.00	–0.136	H–Al_I	0.574	–	1.166
Al(I)	0.95	1.20	0.00	–0.863	Al_I–Al_{II}	0.069	–70.1%	–
Fe(I)	0.44	0.11	7.96	–0.727	H–Fe_I	0.155	–	1.746
					Fe_I–Fe_{II}	0.154	–22.6%	–
					Fe_I–Al_I	0.138	–52.7%	–

[1] OP: Overlap Population
[2] Δ(OP): Overlap Population percentage change.
The geometry distributions of the atoms involved in the bonds are shown in Fig. 1b.

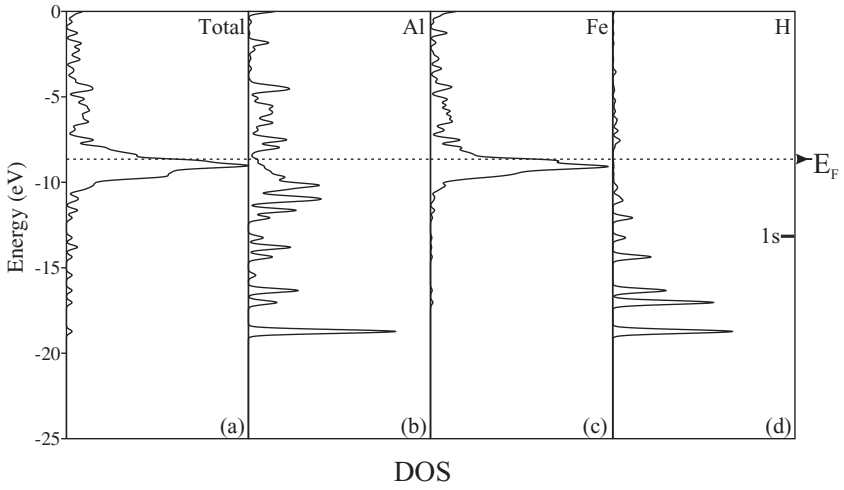

Fig. 4 DOS curves for the B2 FeAl alloy after H absorption at O2: Total (a), Projected DOS on an Al atom (b), on a Fe atom (c) and Projected DOS on H (d). The bar on the right indicates the H 1s-orbital before interaction.

with lower intensity for Al and shifted towards lower energies. The H 1s-level is splitted in several peaks and shifted down below the bottom of the d-band (see Fig. 4d).

The Al–H interaction is developed through several peaks (see Fig. 4b and d). The proximity of the Al 3s-orbital to the H 1s-orbital could be the reason for such interactions. We have also found that the H atom is negatively charged, consistent with the view that the H impurity can be regarded as a screened H-ion in a free electron-like metals [63]. The electron transfer of nearby 0.14 e^- comes from the metal to H.

The overlap population values reveal a metal–metal bond breaking, being the Al–Al bond the most affected. The H bonds mainly with Al and the reported Fe–H OP is much lower than that corresponding in FePd alloys [64] and BCC Fe [65]. The Δ(OP) in Table 1 show that the Al–Al bond is weakened nearly 70% after H absorption, while the Fe–Fe bond is only weakened 23%.

The OPDOS peaks for Fe–Al interaction in Fig. 5 show a decrease in the metal-metal bonding character and two small antibonding interactions at –11.6 eV and –13.8 eV. The Al–H bonding interaction can

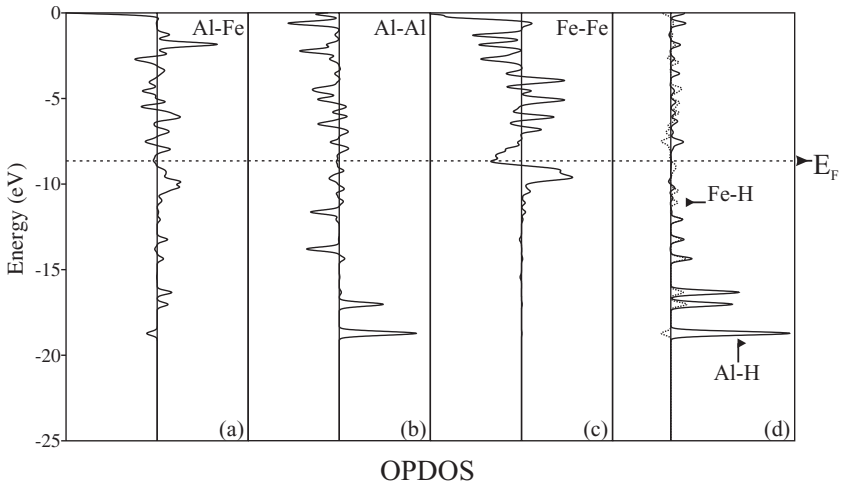

Fig. 5 OPDOS curves of the B2 FeAl alloy after H absorption at O2: Al–Fe (a), Al–Al (b), Fe–Fe (c), and Fe–H (dotted line) and Al–H (solid line) (d).

Table 2 Percentage contributions of the metal orbitals to the Fe–Al, Fe–H and Al–H overlap populations (% OPDOS).

atom	Fe_I (%)																H
	4s		$4p_x$		$4p_y$		$3d_{x2-y2}$		$3d_{z2}$		$3d_{xy}$		$3d_{xz}$		$3d_{yz}$		1s
Al_I 3s	26.06	6.66	–	–	6.57	9.56	0	0	0	0	2.02	1.38	0.44	–	2.02	1.96	63.95
$3p_x$	15.24	28.60	–	–	0.41	0.65	3.01	7.17	0.99	2.10	0.44	0.80	0.20	0.22	5.44	11.09	0.31
$3p_y$	11.57	2.75	–	1.16	–	–	2.70	3.19	0.89	1.88	0.65	1.01	3.46	3.77	0.65	1.09	31.10
$3p_z$	15.24	22.10	–	–	0.41	1.59	0	0	4.04	8.62	5.44	10.43	0.20	0.06	0.44	0.80	4.67
H 1s		45.22	–	–		5.48		15.68		0.13		5.42		31.42		3.48	

be observed in Fig. 5d, with several peaks between –10 eV and –20 eV. The Fe–Fe OPDOS curve presents almost no change (compare Fig. 3c with 5c). The Al–H interaction is higher than Fe–H one (see dotted vs filled lines in Fig. 5d).

The orbital contributions to the metal–metal and H-metal OP are summarized in Table 2. The higher contributions to the metal–metal bonding are the s–s and s–p interactions. After H absorption, the Al–H bond is mainly formed from H 1s-Al 3s (64%) and H 1s–Al $3p_y$ (31%). The Fe–H bond is mainly formed by H 1s–Fe 4s (45%), H 1s–Fe $3d_{xz}$ (31%) and H 1s–Fe $3d_{x^2-y^2}$ (16%).

The change in the orbital contributions to the DOS after H absorption is shown in Fig. 6 for Al and Fig. 7 for Fe. The DOS for Al 3s-orbital present the major change followed by the Al 3p. The Fe 4s shows some peak at lower energy.

In Fig. 8, we have plotted the band structure of the crystal along the symmetry lines $\Gamma \rightarrow X$; $X \rightarrow W$; $W \rightarrow L$; $L \rightarrow \Gamma$. Only parts of the bands are shown in the energy windows. The bands near the Fermi level are formed mainly from transition metal d-states. Three states derived from the metal d-orbitals have t_{eg} symmetry (d_{xy}, d_{yz} and d_{xz}) and are degenerate in Γ [59]. Our calculated band structure is similar to that reported by Das et al. [23] and Li et al. [59]. The effect of the interstitial hydrogen is the introduction of a flat band above 15 eV. Additionally, near the Fermi level the metals bands are modified. Figures 8b–d show the decomposition of the bands in hypothetical Fe, Al and H sub-lattices having the same geometry as in the Fe–Al–H structure.

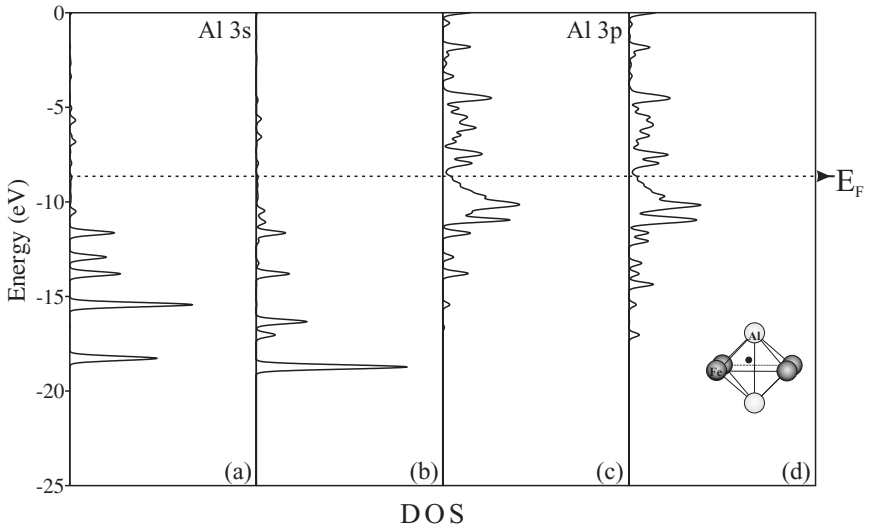

Fig. 6 Projected DOS curves for the Al orbitals before (a, c) and after (b, d) H absorption at O2.

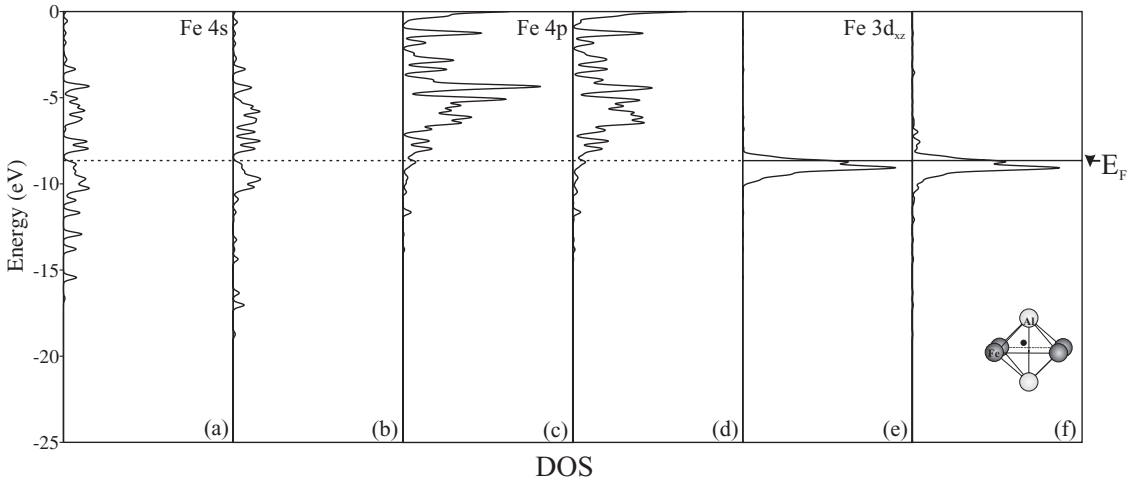

Fig. 7 Projected DOS curves for the Fe orbitals before (a, c, e) and after (b, d, f) H absorption at O2.

5 Conclusions

According to our calculations, the H absorption is a favorable process in the B2 Fe–Al alloy structure. We have analyzed three different environment (tetrahedral (T), Fe (O1) and Al (O2) octahedral). H is stabilized at an Al octahedral interstitial site (O2).

The Al–H distance is shorter than the Fe–H distance and also shorter than that reported for H in bulk Al.

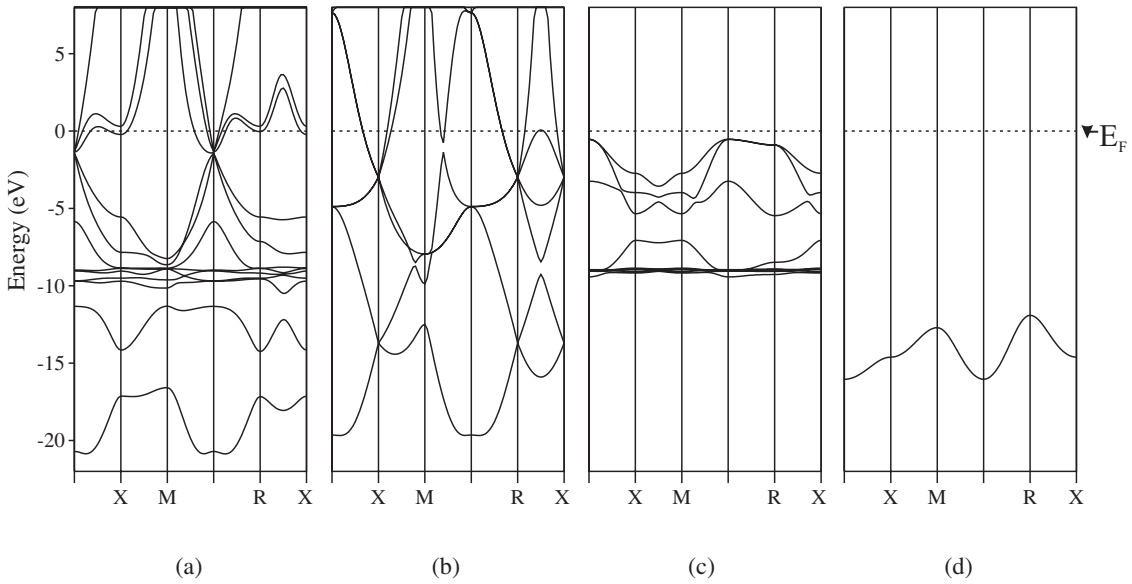

Fig. 8 Band structure of the B2 FeAl alloy with H at O2 plotted along high symmetry directions in an energy window including the Fermi level. The energy scale was plotted relative to E_F. FeAl–H (a), Al (b), Fe (c) and H (d) contributions.

The electronic structure for the pure B2 Fe–Al shows a series of localized sp peaks for the Al–Al bonds and more delocalized for the Fe–Fe bonds. After H absorption, the Al–Al bond is weakening 70% from its initial value, while the Fe–Al bond changes 53%. The Al–H interaction is developed in a series of peaks while a small interaction with Fe is visible.

The Fe–Fe bond is weakened only 15%, a situation that is quite different to the 70% decrease in the bond strength for pure BCC Fe when H is absorbed [56, 60]. It seems that Al protects the Fe–Fe bond and this effect could be suitable to mitigate the well-known phenomena of H embrittlement in low carbon steels.

Acknowledgements Our work was supported by a SeCyT (Argentina) – Akademia of Finland cooperation agreement, UNS-Física and HUT. A.J. and G.B. acknowledge with thanks the hospitality of the Laboratory of Physics of HUT during their on-leave stay at Helsinki. We thank the grants from the Fulbright Commission and the J. S. Guggenheim Foundation. We also thank Dr. K. Johnston for the helpful advice with the calculations and useful suggestions from the reviewers. A.J. and G.B. are members of CONICET. E.A.G. and P.V. J. are fellows of that Institution.

References

[1] D. Fuks, A. Struz, and A. Kiv, Int. J. Quantum Chem. **102**, 606 (2005).
[2] C. G. McKamey, Y. H. DeVan, P. H. Tortprelli, and V. K. Sikka, J. Mater. Res. **6**, 1779 (1991).
[3] I. Baker and P. R. Munroe, Int. Mater. Rev. **42**, 181 (1997).
[4] C. Liu, E. P. George, P. J. Maziasz, and J. H. Schneibel, Mater. Sci. Eng. A **258**, 84 (1998).
[5] W. C. Luu and J. K. Wu, J. Mater. Sci. **35**, 4121 (2000).
[6] R. Balasbramaniam, J. Alloys Compd. **330–332**, 506 (2002).
[7] B. S. J. Kang and R. Cisloiu, Theor. Appl. Fract. Mech. **45**, 25 (2006).
[8] P. R. Munroe and C. H. Kong, Intermetallics **4**, 403 (1996).
[9] J. H. Schneibel, Mater. Sci. Eng. A **258**, 181 (1998).
[10] S. F. Kettle, Physical Inorganic Chemistry: A Coordination Chemistry Approach (Oxford University Press, New York, 2000).
[11] V. N. Antonov, O. V. Krasovka, E. E. Krasovskii, Y. V. Kudryavtsev, V. V. Nemoshkalenko, B. Y. Yavorsky, Y. P. Lee, and K. W. Kim, J. Phys.: Condens. Matter. **9**, 11227 (1997).
[12] S. H. Yang, M. J. Mehl, D. A. Papaconstantopoulos, and M. B. Scott, J. Phys.: Condens. Matter **14**, 1895 (2002).
[13] R. L. Fleischer, D. M. Dimiduk, and H. A. Lipsitt, Annu. Rev. Mater. Sci. **19**, 231 (1989).
[14] R. Besson and J. Morillo, Phys. Rev. B **55**, 193 (1997).
[15] C. L. Fu and M. H. Yoo, Acta Metall. Mater. **40**, 703 (1992).
[16] J. Zou and C. L. Fu, Phys. Rev. B **51**, 2115 (1995).
[17] S. K. Bose, V. Drchal, J. Kudrnovsky, O. Jepsen, and O. K. Andersen, Phys. Rev. B **55**, 8184 (1997).
[18] V. Schott and M. Fähnle, Phys. Rev. B **58**, 14673 (1998).
[19] J. Bogner, W. Steiner, M. Reissner, P. Mohn, P. Blaha, K. Schwarz, R. Krachler, H. Ipser, and B. Sepiol, Phys. Rev. **58**, 14922 (1998).
[20] B. V. Reddy, P. Jena, and S. C. Deevi, Intermetallics **8**, 1197 (2000).
[21] B. V. Reddy, S. C. Deevi, F. A. Reuse, and S. N. Khanna, Phys. Rev. B **64**, 132408 (2001).
[22] B. V. Reddy, S. C. Deevi, A. C. Lilly, and P. Jena, J. Phys.: Condens. Matter **13**, 8363 (2001).
[23] G. P. Das, B. K. Rao, P. Jena, and S. C. Deevi, Phys. Rev. B **66**, 184203 (2002).
[24] P. Mohn, C. Persson, P. Blaha, K. Schwarz, P. Novák, and H. Eschrig, Phys. Rev. Lett. **87**, 196401 (2001).
[25] D. A. Papaconstantopoulus and C. Stephen Hellberg, Phys. Rev. Lett. **89**, 29701 (2002).
[26] F. Lechermann, F. Welsch, C. Elsässer, C. Ederer, M. Fähnle, J. Sanchez, and B. Meyer, Phys. Rev. B **65**, 132104 (2002).
[27] F. Lechermann, M. Fähnle, and J. M. Sanchez, Intermetallics **13**, 1096 (2005).
[28] M. Fähnle, J. Mayer, and B. Meyer, Intermetallics **7**, 315 (1999).
[29] A. Kellou, T. Grosdidier, and H. Aourag, Intermetallics **14**, 142 (2006).
[30] Z. R. Xu and R. B. McLellan, J. Phys. Chem. Solids **61**, 633 (2000).
[31] C. T. Liu, C. L. Fu, E. P. George, and G. S. Painter, ISIJ Int. (Iron Steel Inst. Jpn.) **31**, 1192 (1991).
[32] C. L. Fu and G. S. Painter, J. Mater. Res. **6**, 719 (1991).
[33] C. L. Fu and X. Wang, Mater. Sci. Eng. A **239/240**, 761 (1997).

[34] H. Krimmel, L. Schimmele, C. Elsässer, and M. Fähnle, J. Phys.: Condens. Matter **6**, 7679 (1994).
[35] M. Puska and R. M. Nieminen, Phys. Rev. B **29**, 5382 (1984).
[36] X. Ke, G. J. Kramer, and O. M. Løvvik, J. Phys.: Condens. Matter **16**, 6267 (2004).
[37] D. E. Jiang and E. A. Carter, Phys. Rev. B **70**, 64102 (2004).
[38] P. Hohenberg and W. Kohn, Phys. Rev. **136**, 864 (1964).
[39] W. Koh and L. J. Sham, Phys. Rev. **140**, 1133 (1965).
[40] R. G. Parr and W. Yang, Density Functional Theory of Atoms and Molecules (Oxford University Press, New York, 1989).
[41] Amsterdam Density Functional Package Release 2001 (Vrije Universiteit, Amsterdam).
[42] D. Becke, Phys. Rev. A **38**, 3098 (1988).
[43] C. Lee, W. Yang, and R. G. Parr, Phys. Rev. B **37**, 785 (1988).
[44] R. Ramirez and M. C. Böhm, Int. J. Quantum Chem. **30**, 391 (1986).
[45] R. Ramirez and M. C. Böhm, Int. J. Quantum Chem. **34**, 571 (1988).
[46] M. Hansen, Constitution of Binary Alloys. Metallurgy and Metallurgical Engineering Series (McGraw-Hill Book Co., Inc., USA, 1958).
[47] W. Ekman, Z. Phys. Chem. B **12**, 57 (1931).
[48] A. J. Bradley and A. H. Jay, Proc. R. Soc. Lond. A **136**, 210 (1932).
[49] A. J. Bradley and A. H. Jay, J. Iron Steel Inst. **125**, 339 (1932).
[50] R. Podlucky and A. Neckel, phys. stat. sol. (b) **95**, 541 (1979).
[51] C. Blass, J. Redinger, S. Mannine, V. Honkiäki, K. Hämäläinen, and P. Suortti, Phys. Rev. Lett. **75**, 1984 (1995).
[52] Ch. Müller, H. Wonn, W. Blau, B. Ziesche, and V. B. Krivitskii, phys. stat. sol. (b) **95**, 215 (1979).
[53] B. I. Min, T. Oguchi, H. J. F. Jansen, and A. J. Freeman, J. Magn. Magn. Mater. **54–57**, 1091 (1986).
[54] R. E. Watson and M. Weinert, Phys. Rev. B **58**, 5981 (1998).
[55] D. Nguyen-Manh, D. Mayou, A. Pasturel, and F. Cyrot-Lackmann, J. Phys. F **15**, 1991 (1985).
[56] A. A. Ostroukhov, V. M. Floka, and V. T. Cherepin, Surf. Sci. **352**, 919 (1996).
[57] P. A. Schultz and J. W. Davenport, J. Alloys Compd. **197**, 229 (1993).
[58] N. I. Kulikov, A. V. Postnikov, G. Borstel, and J. Braun, Phys. Rev. B **59**, 6824 (1999).
[59] T. Li, J. W. Morris, and D. Chrzan, Phys. Rev. B **70**, 54107 (2004).
[60] G. A. Botton, G. Y. Guo, W. M. Temmerman, and C. J. Humphreys, Phys. Rev. B **54**, 1682 (1996).
[61] N. Börnsen, G. Beser, B. Meyer, and M. Fähnle, J. Alloys Compd. **308**, 1 (2000).
[62] C. L. Lu and E. Kaxiras, Phys. Rev. Lett. **94**, 155501 (2005).
[63] J. Nørskov, Phys. Rev. B **20**, 446 (1979).
[64] E. Gonzalez, P. Jasen, N. J. Castellani, and A. Juan, J. Phys. Chem. Solids **65**, 25 (2004).
[65] A. Juan and R. Hoffmann, Surf. Sci. **421**, 1 (1999).

